BIOCHEMISTRY
including biophysical chemistry & molecular biology

Article

pubs.acs.org/biochemistry

Structures of *Pseudomonas aeruginosa* LpxA Reveal the Basis for Its Substrate Selectivity

Emmanuel W. Smith,[†] XiuJun Zhang,[†] Cyrus Behzadi,[†] Logan D. Andrews,[‡] Frederick Cohen,[‡] and Yu Chen*[,†]

[†]Department of Molecular Medicine, University of South Florida, 12901 Bruce B. Downs Boulevard, Tampa, Florida 33612, United States

[‡]ACHAOGEN Inc., 7000 Shoreline Court, South San Francisco, California 94080, United States

ABSTRACT: In Gram-negative bacteria, the first step of lipid A biosynthesis is catalyzed by UDP-*N*-acetylglucosamine acyltransferase (LpxA) through the transfer of a *R*-3-hydroxyacyl chain from the acyl carrier protein (ACP) to the 3-hydroxyl group of UDP-GlcNAc. Previous studies suggest that LpxA is a critical determinant of the acyl chain length found in lipid A, which varies among species of bacteria. In *Escherichia coli* and *Leptospira interrogans*, LpxA prefers to incorporate longer *R*-3-hydroxyacyl chains (C14 and C12, respectively), whereas in *Pseudomonas aeruginosa*, the enzyme is selective for *R*-3-hydroxydecanoyl, a 10-hydrocarbon long acyl chain. We now report three *P. aeruginosa* LpxA crystal structures: apo protein, substrate complex with UDP-GlcNAc, and product complex with UDP-3-*O*-(*R*-3-hydroxydecanoyl)-GlcNAc. A comparison between the apo form and complexes identifies key residues that position UDP-GlcNAc appropriately for catalysis and supports the role of catalytic His121 in activating the UDP-GlcNAc 3-hydroxyl group for nucleophilic attack during the reaction. The product-complex structure, for the first time, offers structural insights into how Met169 serves to constrain the length of the acyl chain and thus functions as the so-called hydrocarbon ruler. Furthermore, compared with ortholog LpxA structures, the purported oxyanion hole, formed by the backbone amide group of Gly139, displays a different conformation in *P. aeruginosa* LpxA, which suggests flexibility of this structural feature important for catalysis and the potential need for substrate-induced conformational change in catalysis. Taken together, the three structures provide valuable insights into *P. aeruginosa* LpxA catalysis and substrate specificity as well as templates for future inhibitor discovery.

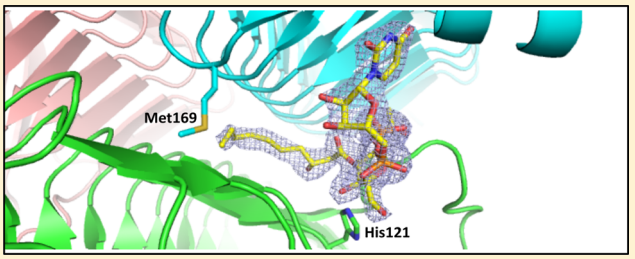

As an opportunistic pathogen, *Pseudomonas aeruginosa* can thrive in a variety of environments and infect many hosts, including humans.[1,2] Serious infections can lead to death and are predominantly hospital-acquired.[2] Furthermore, the pathogen has the ability to acquire resistance to multiple antibiotics through various mechanisms, making infections increasingly difficult to treat.[3−6] Consequently, *P. aeruginosa* has entered the category of superbugs and is of major concern to clinicians, further highlighting the importance of identifying and studying new druggable targets.[5−7]

In *P. aeruginosa*, like most Gram-negative bacteria, lipopolysaccharide (LPS) is a major component of the outer membrane that protects the bacterium from its environment.[8,9] LPS is highly immunogenic and a major virulence factor, and as a result, it is referred to as endotoxin.[10−12] The LPS structure may differ slightly from one bacterium to another, but it is mainly composed of three components: the O-antigen, the core oligosaccharide, and lipid A.[9,13,14] Lipid A is a glucosamine-based phospholipid that anchors lipopolysaccharide to the outer monolayer of the outer membrane.[8,13,15] In *P. aeruginosa*, lipid A is made out of a diglucosamine biphosphate backbone that is linked by O- and N- primary and secondary fatty acids.[9,13] This component is integral to the bacterium's viability and thus has become a desirable target for drug discovery.[16]

The pathway leading to the biosynthesis of lipid A has been well-documented in *Escherichia coli*,[17,18] and it is believed to be conserved across all Gram-negative species. The first step of lipid A biosynthesis involves UDP-*N*-acetylglucosamine (UDP-GlcNAc) acyltransferase (LpxA), which catalyzes the transfer of a *R*-3-hydroxyacyl chain from the *R*-3-hydroxyacyl-acyl carrier protein (ACP) to the glucosamine 3-OH group of UDP-GlcNAc (Figure 1).[16,18] This first step is thermodynamically unfavorable (K_{eq} of ∼0.01 in *E. coli*),[18] but LpxC, the second enzyme in the pathway, catalyzes the committed step through the thermodynamically favored and effectively irreversible deacetylation of UDP-3-*O*-(*R*-3-hydroxyacyl)-GlcNAc (Figure 1).[9,19] The third step is catalyzed by LpxD through the addition of a second *β*-hydroxyacyl chain to make UDP-2,3-diacyl-GlcNAc (Figure 1).[9,20] A series of additional steps results in the production of lipid A, which is attached to the core component of LPS (Figure 1).[8,21] Previous studies have shown that LpxA

Received: June 26, 2015
Revised: September 4, 2015
Published: September 9, 2015

DOI: 10.1021/acs.biochem.5b00720
Biochemistry 2015, 54, 5937−5948

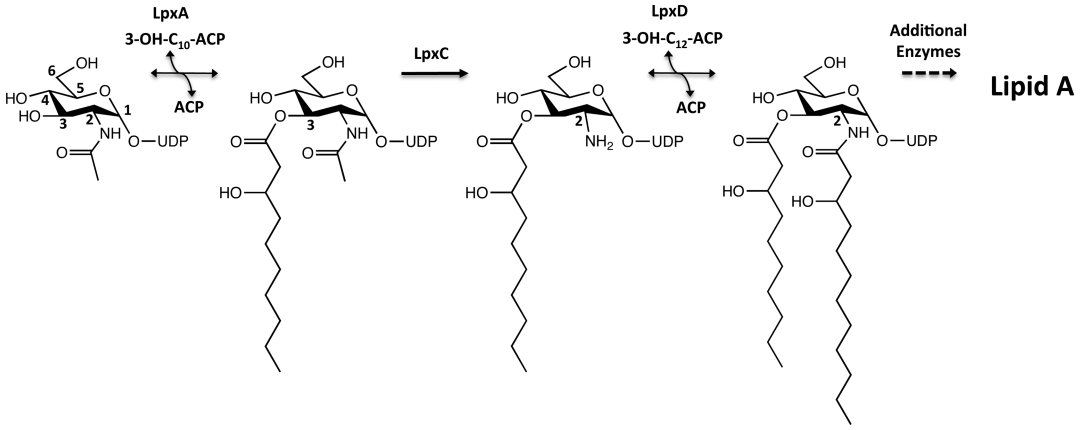

Figure 1. *P. aeruginosa* LpxA catalyzes the first and reversible step of lipid A biosynthesis. LpxA catalyzes the reversible transfer of a hydroxyacyl chain from the ACP protein to the 3-OH position of UDP-GlcNAc. LpxC deacetylates UDP-3-*O*-(*R*-3-hydroxydecanoil)-GlcNAc, and LpxD catalyzes the transfer of a second hydroxyacyl chain from ACP to the 2-NH_2 position. A series of additional enzymes carries out the remaining steps that lead to the biosynthesis of lipid A.

and other enzymes involved in the LPS synthesis pathway provide validated targets for novel antibiotics.[22−25]

LpxA is a soluble cytoplasmic protein that forms a functional homotrimer.[26,27] It shares sequence homology with LpxD, which also forms a homotrimer, unlike LpxC, which is a Zn^{2+}-dependent monomeric enzyme that shares no sequence homology with other deacetylases.[8] Previously solved crystal structures reveal that LpxA forms a left-handed parallel β-helix generated by ∼30 hexapeptide repeats.[28−34] Every turn in the β-helix is made up of a single hexapeptide.[35] Conserved residues, identified previously through sequence alignments, assisted in the identification of the active site, which is located in a cleft formed by the interface of adjacent monomeric units of the trimer. The key catalytic residue, which is conserved across all species, is a histidine that has been proposed to deprotonate the 3-OH of the UDP-GlcNAc substrate, priming it for nucleophilic attack.[36] For this to occur, the 3-OH of UDP-GlcNAc is positioned in the active site near His121 through the formation of multiple hydrogen bonds between the rest of UDP-GlcNAc and other residues. Finally, the acyl chain, carried by the ACP, docks into a hydrophobic cleft and is displaced from the ACP via nucleophilic attack by the 3-OH of UDP-GlcNAc and subsequently attached to UDP-GlcNAc, forming the product, UDP-3-*O*-(*R*-3-hydroxyacyl)-GlcNAc.[9]

LpxA enzymes are selective of their substrate's acyl chain length, but this selectivity varies across species, with some bacteria preferring longer chain hydrocarbons, while other bacteria recognize only shorter chain hydrocarbons.[37−39] In *E. coli*, for example, LpxA catalyzes the transfer of *R*-3-hydroxymyristoyl, a 14C-long fatty acyl chain, from the *R*-3-hydroxymyristoyl-acyl carrier protein (ACP) to UDP-GlcNAc. *In vitro*, *E. coli* LpxA has a catalytic preference for this 14C-long chain over a 10C-long chain by a factor of ∼1000.[39] In *Leptospira interrogans*, LpxA is selective for *R*-3-hydroxylauroyl, a 12C-long fatty acyl chain, which it attaches to the UDP-GlcNAc derivative, UDP-GlcNAc3N.[28] In *P. aeruginosa*, however, LpxA prefers *R*-3-hydroxydecanoyl, a 10C-long *R*-3-hydroxyacyl chain.[39] Lipid A isolates from *E. coli* and *P. aeruginosa* have confirmed incorporation of their specific acyl chains.[9,12] The residues involved in restricting the length of the acyl chains in LpxA were first identified by Wyckoff et al. in *E. coli* and *P. aeruginosa* and named hydrocarbon rulers.[39] These are the amino acids that act as precise measuring tools, allowing the incorporation of hydrocarbon chains of very specific lengths; longer chains are disallowed, whereas shorter chains do not provide sufficient hydrophobic interactions and therefore lose significant affinity. Structural studies have shown that in *E. coli* LpxA, His191 is implicated in restricting the chain length to be 14C,[35] whereas in *L. interrogans* LpxA, structural studies have shown that Lys171 serves a similar purpose for the shorter 12C chain.[28] In *P. aeruginosa* LpxA, Met169 has been functionally identified as the hydrocarbon ruler, denying longer chain hydrocarbons from binding.[39] Furthermore, it has been shown that this selectivity can be switched *in vitro* and *in vivo* between *E. coli* LpxA and *P. aeruginosa* LpxA through reciprocal mutations of G173M and M169G, respectively.[39] Until now, however, the structure of *P. aeruginosa* has been lacking, so a comprehensive understanding of how this selectivity is accomplished by Met169 was incomplete.

Here, we report the first structures of *P. aeruginosa* LpxA in three forms: apo protein at 1.81 Å, substrate complex with UDP-GlcNAc at 2.16 Å, and product complex with UDP-3-*O*-(*R*-3-hydroxydecanoyl)-GlcNAc at 2.30 Å. These structures have unambiguously identified the active site and provide detailed information on the residues that orient UDP-GlcNAc for catalysis, including the role of His121 as a general base, and on how Met169 confers *P. aeruginosa* LpxA with its exceptional selectivity for *R*-3-hydroxydecanoyl, the 10C-long hydrocarbon chain, thus serving as the hydrocarbon ruler. Such structural information is not only of significance for better understanding substrate recognition and catalysis in this class of enzymes but also for aiding in the development of inhibitors using a structure-based approach.

EXPERIMENTAL PROCEDURES

Materials. All reagents and chromatography supplies were purchased from Fisher Scientific. Crystal screens were purchased from Qiagen. UDP-GlcNAc was purchased from Sigma-Aldrich. The LpxA product, UDP-3-*O*-(*R*-3-hydroxydecanoyl)-GlcNAc, was synthesized by the Alberta Research Council (Alberta, Canada)

Purification of Recombinant LpxA. The plasmid pET28b containing the N-terminal His-tagged *P. aeruginosa* LpxA sequence was transformed into Rosetta (DE3) pLysS cells (Novagen). The cells were incubated in LB media supplemented with 35 μg/mL chloramphenicol and 50 μg/mL

DOI: 10.1021/acs.biochem.5b00720
Biochemistry 2015, 54, 5937−5948

Table 1. Data Collection and Refinement Statistics

	LpxA apo	LpxA/UDP-GlcNAc	LpxA/UDP-3-*O*-(*R*-3-hydroxydecanoyl)-GlcNAc
Data Collection			
space group	$P2_12_12_1$	$P2_12_12_1$	$P2_12_12_1$
cell dimensions: *a*, *b*, *c* (Å)	79.03, 82.18, 220.51	80.04, 83.56, 222.43	79.96, 83.33, 220.37
resolution range (Å)	110.26−1.81 (1.84−1.81)[a]	111.21−2.16 (2.20−2.16)[a]	110.18−2.30 (2.34−2.30)[a]
$\langle I\rangle/\langle\sigma(I)\rangle$	38.5 (2.3)[a]	13.1 (2.1)[a]	26.3 (2.2)[a]
completeness (%)	98.8 (97.8)[a]	98.4 (99.5)[a]	98.5 (98.1)[a]
R_{merge}	0.036 (0.770)[a]	0.066 (0.755)[a]	0.051 (0.580)[a]
redundancy	7.5 (7.6)[a]	6.2 (6.3)[a]	6.4 (6.3)[a]
Refinement			
no. of reflections used	122 365	75 873	57 656
R_{work}	0.184	0.177	0.193
R_{free}	0.211	0.226	0.245
no. of atoms			
protein/ligands/water	11 832/5/816	11 800/254/411	11 663/209/231
root-mean-square deviations			
bond lengths (Å)	0.0117	0.0115	0.0186
bond angles (deg)	1.3973	1.5581	1.8159
average B-factor (Å^2)			
protein/ligands/water	24.1/39.8/30.3	33.9/47.5/36.4	32.4/29.5/28.3
Ramachandran plot statistics[b]			
most favored (%)	87.4	87.1	86.7
additional allowed (%)	11.7	12.3	12.1
generously allowed (%)	1.0	0.7	1.2
PDB code	5DEM	5DEP	5DG3

[a]Numbers in parentheses are for the highest resolution shell. [b]Ramachandran plot statistics were calculated with ProCheck V 3.4.4 from the PDB validation server.

kanamycin at 37 °C overnight. The overnight culture was then diluted into 1 L of LB media containing 35 μg/mL chloramphenicol and 50 μg/mL kanamycin at 1:100 and incubated at 37 °C until the OD_{600} reached 0.6−0.8. The protein expression was initiated with 0.5 mM IPTG, and incubation continued at 37 °C for an additional 4 h. The cells were harvested by centrifugation at 5000*g* for 10 min. The pellet was resuspended in buffer A (20 mM Tris-HCl, pH 8.4, 250 mM NaCl, 20 mM imidazole, and 10% glycerol). The cells were disrupted by sonication, followed by centrifugation at 35 000*g* for 40 min to remove debris. The supernatant was then loaded to a HisTrap affinity column. The protein was eluted with a linear gradient of 500 mM imidazole. The fractions containing the tagged LpxA were pooled and concentrated. The sample was loaded to a HiLoad 16/60 Superdex 75 column for further purification in thrombin cleavage buffer (20 mM Tris, pH 8.4, 150 mM NaCl, and 10% glycerol). The peak fractions containing the His-tagged LpxA were pooled, and the concentration of the protein was determined by OD_{280}. The protease thrombin (Roche) was added at a ratio of one unit per milligram of the protein. After overnight incubation at room temperature, the samples were then loaded onto a HisTrap column to remove any uncleaved protein. The flow-through was collected and concentrated, followed by gel filtration with the HiLoad 16/60 Superdex 75 column. The protein eluted at a peak consistent with the size of the trimeric form. The untagged LpxA was stored at −80 °C at 14.3 mg/mL concentration in a buffer containing 20 mM potassium phosphate (pH 8.6) and 250 mM NaCl. The purity of the protein was determined by SDS-PAGE to be >95%.

LpxA Crystallization. Qiagen crystallization screens JCSG suites I−IV, $AmSO_4$, MPD, Core I and II, were screened using a Phoenix nanodispenser, and 0.2 and 0.4 μL aliquots of protein solution (14.3 mg/mL), each with 0.2 μL of well solution, were used to search for crystallization conditions. *P. aeruginosa* LpxA readily crystallized under many conditions, producing cuboidal crystals of poor X-ray diffraction quality. Crystals with an almond-like morphology emerged in 0.1 M imidazole, pH 8.0, 20% (w/v) PEG 1000, and 0.2 M calcium acetate, which diffracted to high resolution. The crystals appeared within 2−4 days and measured up to 0.1 mm in length.

The apo crystal was soaked in crystallization buffer containing 25% glycerol and cryocooled in liquid nitrogen. The UDP-GlcNAc complex was obtained by transferring apo crystals into crystallization solution containing 50 mM UDP-GlcNAc and soaking overnight, whereas the UDP-3-*O*-(*R*-3-hydroxydecanoyl)-GlcNAc complex was obtained by transferring apo crystals into crystallization solution containing 10 mM UDP-3-*O*-(*R*-3-hydroxydecanoyl)-GlcNAc and soaking over a period of 3 days. The crystals were then briefly soaked in crystallization buffer containing 25% glycerol and ligand and then immediately cryocooled in liquid nitrogen.

Data Collection and Structure Determination. X-ray diffraction data for the apo and UDP-3-*O*-(*R*-3-hydroxydecanoyl)-GlcNAc complex LpxA crystals were collected at the SER-CAT ID beamline at the Advanced Photon Source (APS) at Argonne National Laboratory. X-ray diffraction data for the UDP-GlcNAc complex LpxA crystal was collected at the 8.3.1 beamline at the Advanced Light Source (ALS) at Lawrence Berkeley National Laboratory. For all three data sets, indexing, integration, and scaling was done through HKL2000.[40] The apo structure was solved via molecular replacement in MolRep[41] (CCP4 suite)[42] using a homology model constructed through Modeller,[43] which was based on the *E. coli* LpxA structure (PDB ID: 2AQ9).[24] Model rebuilding was carried out using the program COOT,[44] and refinement was performed using

DOI: 10.1021/acs.biochem.5b00720
Biochemistry 2015, 54, 5937−5948

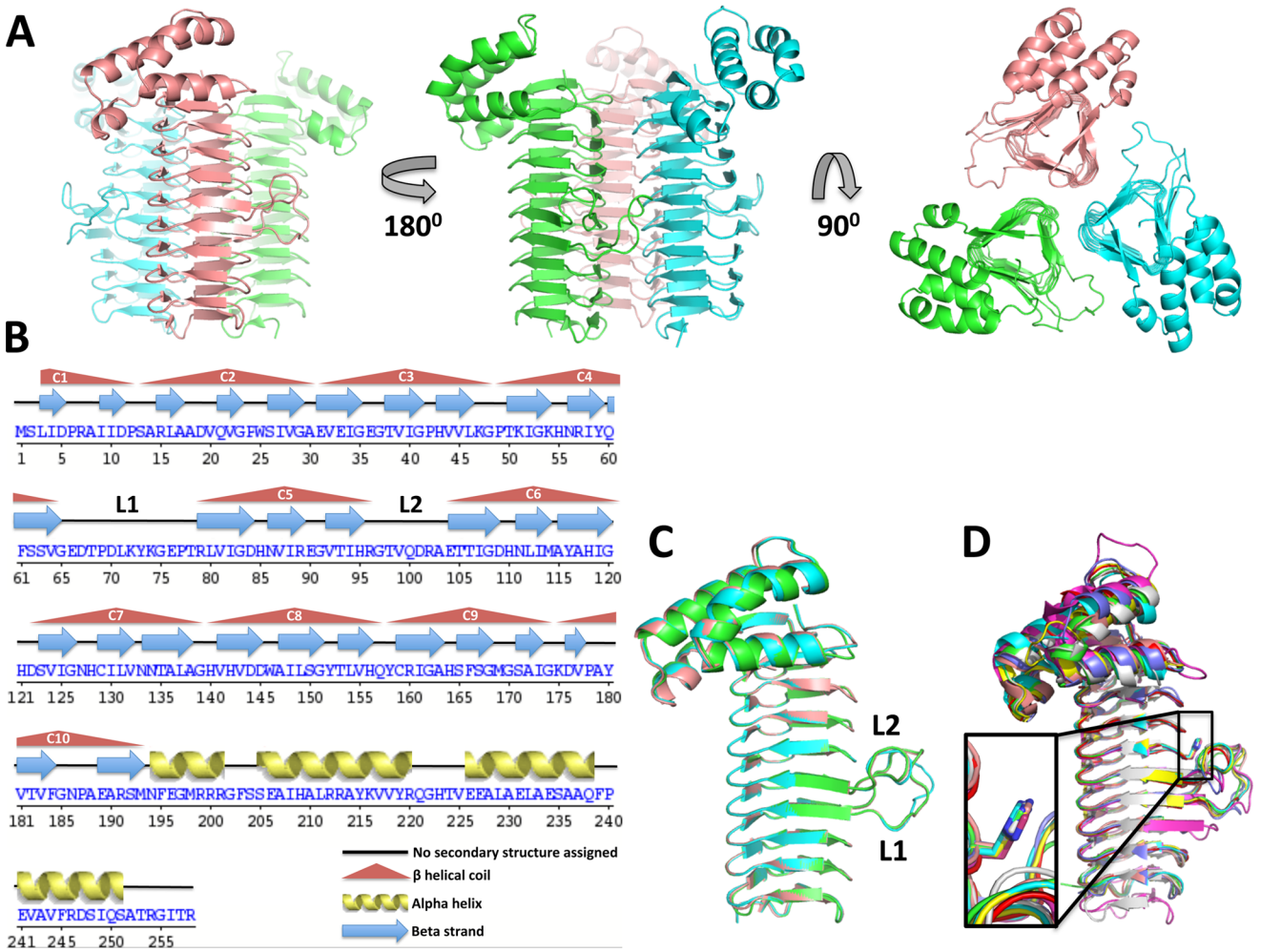

Figure 2. *P. aeruginosa* LpxA apo crystal structure. (A) The biologically relevant homotrimer contained within the asymmetric unit seen from two side views and one top view. (B) Diagram of the secondary structure. (C) Superimposition of all three monomers from the biologically relevant homotrimer, showing loops L1 and L2. (D) *P. aeruginosa* LpxA monomer superimposed onto eight ortholog LpxA monomeric structures (*E. coli* (PDB ID: 1LXA), *B. thailandensis* (PDB ID: 4EQY), *A. baumannii* (PDB ID: 4E6U), *L. interrogans* (PDB ID: 3HSQ), *H. pylori* (PDB ID: 1J2Z), *A. thaliana* (PDB ID: 3T57), *C. jejuni* (PDB ID: 3ROS), and *B. fragilis* (PDB ID: 4R36)). Superimposition shows high structural similarity, the highly conserved catalytic histidine, and some variation in flexible loop regions and α-helical domains.

Phenix[45] and Refmac5[46] (CCP4 suite).[42] The complex structures were subsequently solved via molecular replacement using the apo structure as a template. Figures of protein structures were made using PyMOL.[47] The omit map (Figure 7C) was created in Phenix[45] by omitting target regions and refining with simulated annealing to decrease model bias. Data collection and refinement statistics for all three structures are presented in Table 1. The protein coordinates have been deposited into the Protein Data Bank with accession codes 5DEM for the apo protein, 5DEP for the substrate complex with UDP-GlcNAc, and 5DG3 for the product complex with UDP-3-*O*-(*R*-3-hydroxydecanoyl)-GlcNAc.

RESULTS AND DISCUSSION

Apo Structure. The *P. aeruginosa* LpxA apo structure was solved at 1.81 Å resolution and belongs to the $P2_12_12_1$ space group (Table 1). Each asymmetric unit contains six monomers. Three of those monomers form a biologically relevant homotrimer through a noncrystallographic 3-fold symmetry (Figure 2A). The remaining three monomers in the asymmetric unit also form functional homotrimers, but they do so with monomers from adjacent asymmetric units. The conformation of each monomer is virtually identical, and when they are superimposed to monomer A, they have an average RMSD value of 0.193 Å, aligning an average of 1480 atoms. Superimposition of all of the monomers in the biologically relevant trimer shows negligible structural variation, except at the more flexible loop region L1 (Glu66−Thr78), where differences are observed (Figure 2B,C). *P. aeruginosa* LpxA contains high overall structural similarity to other previously solved LpxA structures, such as *E. coli* (54% sequence identity)[30] and *L. interrogans* (41% sequence identity),[28] yet it also displays differences in residue composition and side chain conformations, especially in flexible loop regions, where backbone variations are observed (Figure 2D).

The amino acids in the apo structure were clearly resolved in the electron density map, with the exception of Met1 (chains A−F) and Ser2 (chain C). The structure of *P. aeruginosa* LpxA, similar to orthologs in other bacteria, is made up of two distinct domains: an N-terminal β-strand domain and a C-terminal α-helical domain (Figure 2B,C). Ten β-helical coils form the typical LβH (left-handed parallel beta-helix) domain of the N-terminus, a motif common in enzymes with acyltransferase activity.[20] Starting at Met1 and ending at Met193, this coiled

DOI: 10.1021/acs.biochem.5b00720
Biochemistry 2015, 54, 5937−5948

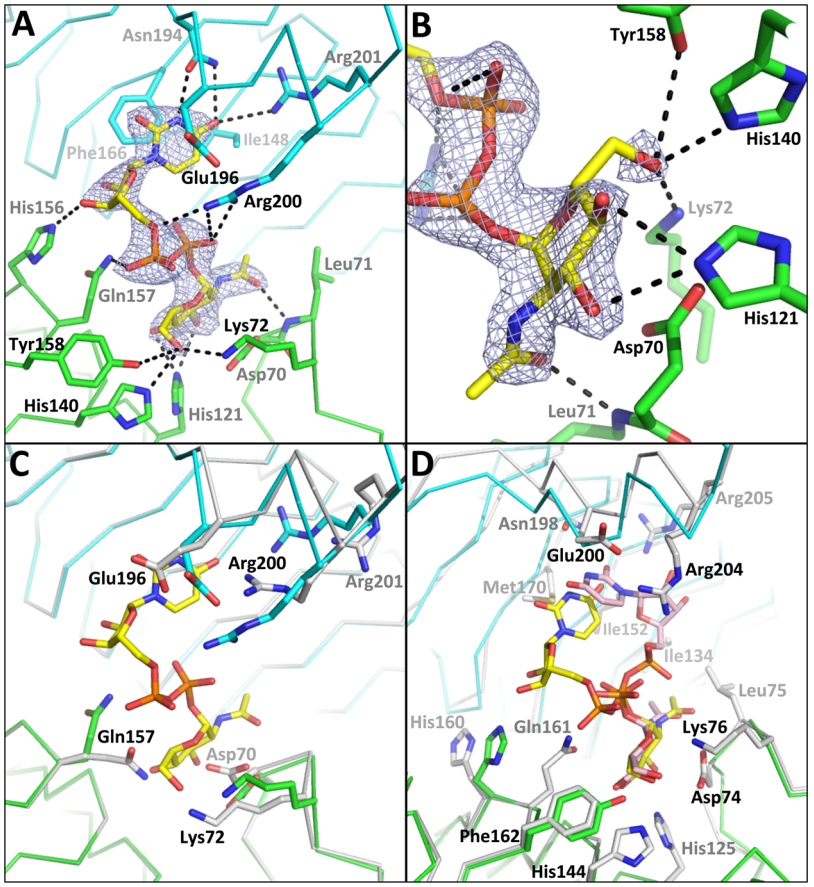

Figure 3. UDP-GlcNAc bound to *P. aeruginosa* LpxA active site. Monomers A and B of the *P. aeruginosa* complex are colored cyan and green, respectively, whereas the substrate is yellow. Hydrogen-bonding interactions in the active site at the dimer interface are represented by dotted lines. (A) The unbiased $F_o - F_c$ map (contoured at 3.0σ) unambiguously identifies the binding pose of UDP-GlcNAc in the active site. Uracil and phosphate moieties interact with monomer A (cyan), whereas ribose, phosphate, and glucosamine moieties interact with monomer B (green). (B) Details of the interactions between the glucosamine moiety and monomer B. The 3-OH group is within hydrogen-bond distance to catalytic residue His121. (C) Comparison of *P. aeruginosa* LpxA/UDP-GlcNAc complex to apo *P. aeruginosa* LpxA (light gray) showing only residue side chains that demonstrate conformational changes upon binding UDP-GlcNAc. (D) Comparison of *P. aeruginosa* LpxA/UDP-GlcNAc complex to *E. coli* LpxA/UDP-GlcNAc complex (light gray) showing the residues that orchestrate UDP-GlcNAc binding on *E. coli* LpxA. His156 and Tyr158 of *P. aeruginosa* LpxA are also shown but are not labeled (*P. aeruginosa* ligand (yellow)/*E. coli* ligand (light pink)). Residue labels are based on *E. coli* LpxA sequence.

motif consists mostly of hexapeptide repeats, giving rise to 29 distinct β-strands (Figure 2B). Every three β-strands form one complete β-helical coil, creating the appearance of an equilateral triangle. Side chains in the coil hexapeptides alternate between those facing internally and those facing externally. Those facing internally establish polar and nonpolar interactions, further rigidifying the structure.

Two loops, L1 (Glu66–Thr78) and L2 (Arg96–Ala103), extend out of the LβH domain at coils C4–C5 and C5–C6, interrupting the β-helical motif (Figure 2B,C). These loops show slight conformational variation among different monomers in the asymmetric unit (Figure 2C) and display structural variations between orthologs in other bacteria (Figure 2D).

Immediately following the LβH domain, a series of four consecutive α-helices of different lengths and tilts is formed, starting at Asn194 and extending all the way to the C-terminus (Figure 2B,C). This α-helical domain shows some conformational variation among ortholog proteins from other bacterial and plant species (Figure 2D).[28−33] While *P. aeruginosa* LpxA is most similar to the *E. coli* LpxA (PDB ID: 1LXA),[30] there seems to be some variation at the C-terminal end of the third α-helix, involving different tilts compared to those of bacterial orthologs *Acinetobacter baumannii* (PDB ID: 4E6U),[29] *L. interrogans* (PDB ID: 3HSQ),[28] *Campylobacter jejuni* (PDB ID: 3R0S), *Burkholderia thailandensis* (PDB ID: 4EQY),[32] *Helicobacter pylori* (PDB ID: 1J2Z),[31] and *Bacteroides fragilis* (PDB ID: 4R36)[34] and plant ortholog *Arabidopsis thaliana* (PDB ID: 3T57).[33]

The catalytic site in the biologically relevant trimer lies in the protein−protein interface where coils C6−C9 from adjacent monomers meet. Therefore, each biologically relevant trimer contains three catalytic sites. Even though there are some differences in active site residues among different orthologs, key catalytic residues, such as His121 in *P. aeruginosa* LpxA, are conserved across all species (Figure 2D). This suggests the same mode of catalysis but perhaps variation in ligand positioning and substrate specificity among orthologs.

LpxA/UDP-GlcNAc Substrate Complex. The *P. aeruginosa* LpxA/UDP-GlcNAc complex structure, obtained by soaking the substrate compound into the LpxA apo crystal, was solved at 2.16 Å resolution (Table 1). The resulting electron density unambiguously identified the presence and localization of six UDP-GlcNAc molecules within the asymmetric unit, three of which appear in the active site at the protein−protein interface. Only one of those three is at an active site contained within the asymmetric unit (Figure 3),

DOI: 10.1021/acs.biochem.5b00720
Biochemistry 2015, 54, 5937−5948

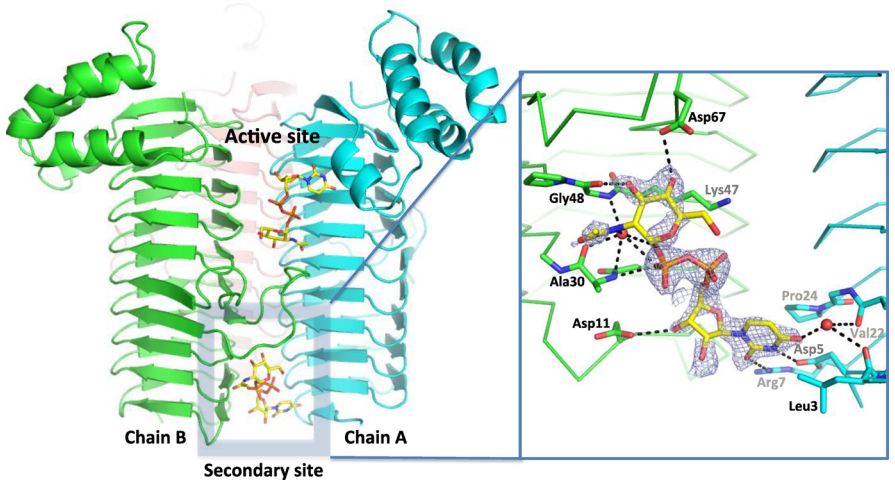

Figure 4. UDP-GlcNAc observed at a secondary binding site at the dimer interface. Monomers A and B of the *P. aeruginosa* complex are colored cyan and green, respectively, whereas the substrates are yellow. A UDP-GlcNAc molecule is bound outside the active site on the N-terminal side of loop L1 at the same dimer interface. Potential hydrogen bonds between UDP-GlcNAc and LpxA are depicted as black dotted lines. Water molecules are represented as red spheres.

whereas the other two are at active sites formed at the crystal-packing interface together with monomers from adjacent asymmetric units. For these two ligands, applying crystallographic symmetry yields the complete active site and identifies all protein−ligand interactions, confirming that all three molecules bind in an identical manner to the active site. Electron density for the remaining UDP-GlcNAc molecules was observed outside the active site at three distinct sites. One of them is positioned near monomer C directly at the cleft where α-helix 1 and the β-strand domain meet. Only two potential hydrogen-bond interactions are possible for this binding pose, and the electron density for the GlcNAc moiety of the substrate is not well-defined, indicating conformational disorder. This suggests that this binding pose is a crystal-packing artifact. The other two molecules, however, are positioned at the protein−protein interface, but they are at a site situated below the active site, on the N-terminal side of loop L1 (Figure 4). One of these two molecules binds at the protein−protein interface within the asymmetric unit (below the active site) (Figure 4), whereas the other is positioned at a protein−protein interface comprised by monomers from adjacent asymmetric units, yet the binding poses of both molecules are nearly identical when crystallographic symmetry is applied. At this secondary site, the ligand establishes many favorable polar and nonpolar interactions with residues from both monomers at the protein−protein interface within the biological homotrimer (Figure 4). Cumulatively, these interactions are fewer than the interactions observed at the biologically relevant active site (Figure 3A,B), but they are still plentiful enough to possibly contribute to binding *in vivo*, increasing the local concentrations of the substrate near the protein active site. The residues interacting with the ligand are not conserved, but it would be of interest to test whether this could be a biologically relevant secondary site unique to *P. aeruginosa* LpxA or is simply a crystal-packing artifact. However, the focus hereinafter will be on the active site formed within the asymmetric unit at the protein−protein interface between monomers A and B (Figure 3).

UDP-GlcNAc interacts with the active site mostly through polar interactions with residues from both monomers A and B (Figure 3A). The uracil moiety and certain atoms of the diphosphate moiety hydrogen bond to monomer A (Figure 3A), whereas the ribose, GlcNAc, and other atoms of the diphosphate moieties interact with monomer B (Figure 3A,B). On the one end of the UDP-GlcNAc molecule, the 3-N and 4-O atoms of uracil are within hydrogen-bond distance to Asn194/Oδ1 and Asn194/Nδ2 (chain A), respectively. The 4-O atom of uracil is also within hydrogen-bond distance to Arg201/Nη2 (Figure 3A). The remaining nonpolar atoms of the uracil ring appear to lie against the aromatic side chain of Phe166 (chain A), which also forms van der Waals contacts with two carbon atoms on the ribose ring. Van der Waals contacts also form between the uracil ring and Ile148 on one side, as well as with the apolar side chain atoms of Glu196 on the other side. The 3′-OH of the ribose moiety hydrogen bonds with His156/Nε2 (chain B), whereas the remaining polar atoms of the ribose appear to interact only with the solvent. Arg200/Nη2 (chain A) interacts with the linker-O atom of α-phosphate and Arg200/Nη1 with an O atom of the β-phosphate (Figure 3A), whereas an α-phosphate O atom is within hydrogen-bond distance to Gln157/Nε2 (chain B) (Figure 3A). Meanwhile, the GlcNAc moiety appears to implicate an abundance of hydrogen bonds with residues of chain B (Figure 3A,B). The GlcNAc 6-OH hydrogen bonds with a series of polar atoms, such as Tyr158/Oη, His140/Nε2, and Lys72/Nζ (Figure 3B). The 3-OH group of GlcNAc is within hydrogen-bond distance to the proposed catalytic base His121/Nε2 (chain B), which is believed to function by deprotonating 3-OH and priming it for nucleophilic attack (Figure 3B). The 4-OH group of GlcNAc is also within hydrogen-bond distance to His121/Nε2, but it is at a less favorable angle than the 3-OH group. Lastly, the acetyl O atom hydrogen bonds with the backbone Leu71/N atom (Figure 3B). The apolar atoms of the Asp70 side chain form van der Waals contacts with the apolar atoms of the GlcNAc moiety, whereas the Leu71 side chain appears to be within van der Waals distance to the apolar side of the acetyl group (Figure 3A).

Comparison of the LpxA apo structure to the LpxA/UDP-GlcNAc complex shows the conformational changes that are induced upon binding the substrate (Figure 3C). Gln157 (chain B) has flipped away from the pocket to make room for the ligand and to hydrogen bond with the α-phosphate,

DOI: 10.1021/acs.biochem.5b00720
Biochemistry 2015, 54, 5937−5948

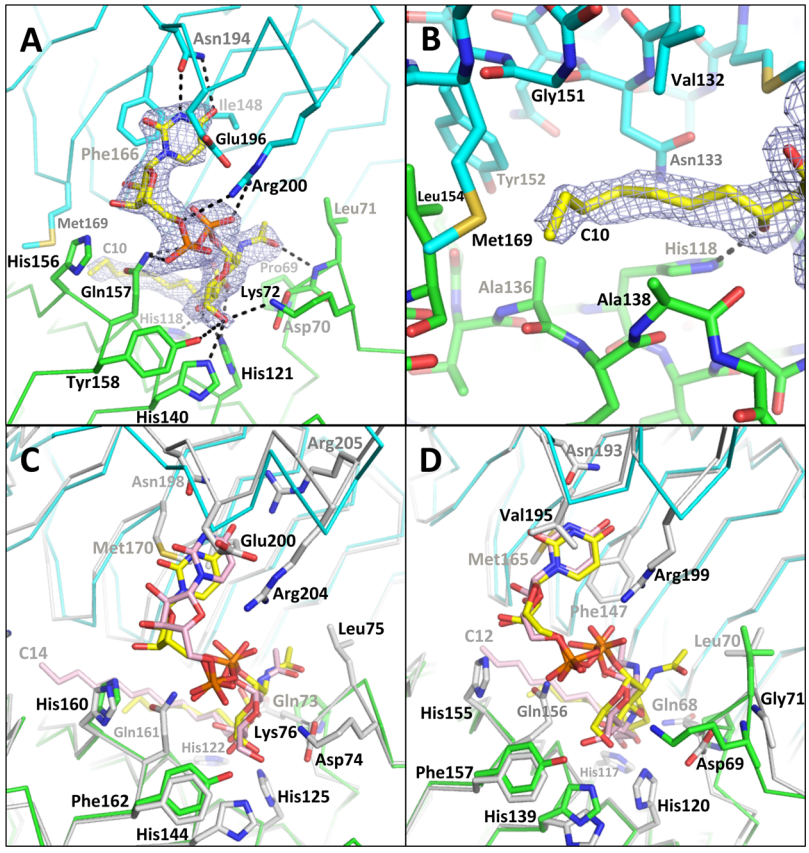

Figure 5. UDP-3-*O*-(*R*-3-hydroxydecanoyl)-GlcNAc bound to *P. aeruginosa* LpxA active site. Monomers A and B of the *P. aeruginosa* complex are colored cyan and green, respectively, whereas the product is yellow. (A) The unbiased $F_o - F_c$ map (contoured at 3.0σ) unambiguously identifies the binding pose of UDP-3-*O*-(*R*-3-hydroxydecanoyl)-GlcNAc in the active site. (B) Details of the binding of the acyl chain in the hydrophobic cleft. (C) Comparison of *P. aeruginosa* LpxA/UDP-3-*O*-(*R*-3-hydroxydecanoyl)-GlcNAc complex to *E. coli* LpxA/UDP-3-*O*-(*R*-3-hydroxymyristoyl)-GlcNAc complex (light gray) showing the residues that orient the ligand in *E. coli* LpxA (*E. coli* ligand in light pink). His156 and Tyr158 of *P. aeruginosa* LpxA are also shown but are not labeled. Residue labels are based on *E. coli* LpxA sequence. (D) Comparison of *P. aeruginosa* LpxA/UDP-3-*O*-(*R*-3-hydroxydecanoyl)-GlcNAc complex to the *L. interrogans* LpxA/product complex (light gray) showing the residues that orient the ligand in *L. interrogans* LpxA and also highlighting residues in chain B of *P. aeruginosa* LpxA that help to explain differences in ligand pose between the two orthologs (*L. interrogans* ligand in light pink). Residue labels are based on *L. interrogans* LpxA sequence. Leu71, Lys72, His140, and Tyr158 of *P. aeruginosa* LpxA are also shown but are not labeled.

whereas Lys72 (chain B) moves in to interact with the GlcNAc moiety (Figure 3C). Asp70 (chain B) also moves away from the pocket to accommodate the ligand and allow the nonpolar atoms of its side chain to provide a hydrophobic surface for the apolar atoms of the GlcNAc moiety (Figure 3C). On chain A, both Arg200 and Arg201 adopt alternative conformations in the complex structure by moving closer to interact with UDP-GlcNAc (Figure 3C). Finally, Glu196 moves away from the pocket to accommodate the ligand and to also provide additional apolar surface for the uridine moiety (Figure 3C). Due to these interactions between UDP-GlcNAc and chain A, the entire Asn194−Ser205 backbone segment of chain A is pulled closer toward the ligand in the complex structure compared to that in the apo form (Figure 3C).

Currently in the PDB, there is an *E. coli* ortholog LpxA structure complexed with UDP-GlcNAc (PDB ID: 2JF3).[48] The *E. coli*/UDP-GlcNAc complex structure contains one monomer per asymmetric unit. By applying crystallographic symmetry operations and superimposing the *E. coli* complex to the *P. aeruginosa* LpxA complex structure, direct comparison of the binding pose of UDP-GlcNAc between these two orthologs demonstrates both significant differences and similarities in UDP-GlcNAc binding (Figure 3D). The biggest difference lies in the positioning of the uridine moiety, which is flipped around the phosphate-O linker bond, when comparing the two complexes (Figure 3D). This conformational difference may have resulted from variations in the interactions between the protein and the substrate. Some potential hydrophobic interactions, like the ones observed between UDP-GlcNAc and Phe166 (chain A), are not present in the *E. coli* complex, since the equivalent Met170 would be unable to establish the same interactions with both the uracil and ribose groups. Also, even though His156 (chain B), which interacts with the ribose moiety in *P. aeruginosa* LpxA, is conserved between these two orthologs, in the *E. coli* complex the equivalent His160 does not interact with the ribose but instead is flipped away from the ligand and occupies a space normally held by Met169 in the *P. aeruginosa* LpxA (Figure 3D). Another reason why the alternative uridine moiety conformation is observed may be due to the slightly wider binding site that accommodates the uridine moiety in the *E. coli* LpxA. This difference is especially noticeable when the *E. coli* and *P. aeruginosa* orthologs are superimposed, where chain A in *P. aeruginosa* is shifted closer toward the ligand, making the pocket narrower (Figure 3D), and, as a consequence, the alternative uridine moiety conformation would have been obstructed by residue Ile148

DOI: 10.1021/acs.biochem.5b00720
Biochemistry 2015, 54, 5937−5948

(Ile152 in *E. coli*). On the other hand, while the position of the α-phosphate is different in these two binding poses, the position of the β-phosphate is quite similar, and even more so is the positioning of the GlcNAc moiety. Therefore, the hydrogen-bonding network between the GlcNAc moieties in these two complexes is very similar. An exception is that Tyr158 in *P. aeruginosa* LpxA is Phe162 in *E. coli* LpxA (Figure 3D) and is thus incapable of hydrogen bonding to 6-OH of GlcNAc.

In addition to the *E. coli* LpxA-UDP-GlcNAc complex, there is another most recent UDP-GlcNAc complex crystal structure with the *B. fragilis* LpxA ortholog (PDB ID: 4R37).[34] In the *B. fragilis* LpxA complex, the substrate shows a binding pose that is nearly identical to that of the *P. aeruginosa* complex, whereas the binding site, like in the *P. aeruginosa* LpxA complex, is also narrower than that in the *E. coli* structure. Cumulatively, the structural information obtained from all three ortholog complex structures further supports that the mechanism of catalysis is conserved.

LpxA/UDP-3-*O*-(*R*-3-hydroxydecanoyl)-GlcNAc Product Complex. The *P. aeruginosa* LpxA/UDP-3-*O*-(*R*-3-hydroxydecanoyl)-GlcNAc complex structure was solved at 2.30 Å resolution (Table 1). Electron density for the product was observed in four of the six active sites associated with the asymmetric unit, compared to only three active sites occupied in the LpxA/UDP-GlcNAc complex structure. Extensive hydrophobic contacts of the product within the acyl chain binding site may help to explain why the UDP-GlcNAc substrate was found in only three active sites compared to the four products found in the product complex. Addition of the acyl chain also appears to prevent the product from being accommodated at the noncatalytic sites where the substrate was found. Superimposition of the four molecules shows negligible conformational variation; thus, the focus hereafter will be at the active site formed between chains A and B (Figure 5).

The unbiased $F_o - F_c$ map unambiguously identifies the binding pose of UDP-3-*O*-(*R*-3-hydroxydecanoyl)-GlcNAc at the A−B chain interface, which shares striking similarities with the substrate complex in this region (Figure 5A). The UDP-GlcNAc moiety is engaged in the same hydrogen-bonding network as that seen in the substrate complex (Figures 3A and 5A). The acylated 3-O of the GlcNAc moiety is positioned similarly to the GlcNAc 3-OH of the substrate, and the acyl chain extends from there into the acyl chain binding cleft (Figure 5A,B). His118/Nε2 appears within hydrogen-bond distance to the acyl chain hydroxyl, which might help to anchor the chain into the hydrophobic cavity (Figure 5B). The acyl chain establishes multiple hydrophobic contacts with the protein. Apolar atoms of the acyl chain complement the hydrophobic tunnel formed by chain A residues Val132, Tyr152, Met169, the nonpolar side chain atoms of Asn133, and the backbone of Gly151, as well as chain B residues Ala136, Ala138, and Leu154 (Figure 5B).

Structures of *E. coli* and *L. interrogans* LpxA complexed to their acylated UDP-GlcNAc products have been previously solved: the *E. coli* LpxA is in complex with UDP-3-*O*-(*R*-3-hydroxymyristoyl)-GlcNAc, a 14C-long chain product (PDB ID: 2QIA),[35] and the *L. interrogans* LpxA is in complex with its 12C-long acyl chain product (PDB ID: 3I3X).[28] Superimposition of our *P. aeruginosa* LpxA complex structure to the *E. coli* LpxA complex shows that UDP-3-*O*-(*R*-3-hydroxymyristoyl)-GlcNAc binds to *E. coli* LpxA in an orientation similar to how UDP-3-*O*-(*R*-3-hydroxydecanoyl)-GlcNAc binds to *P. aeruginosa* LpxA (Figure 5C), with only minor differences. The most noticeable difference is observed in the slight shift of the uridine moiety toward chain A in *E. coli*, probably as a result of the slightly wider binding site in *E. coli* LpxA. Even though His160 in *E. coli* LpxA adopts the same conformation as His156 in *P. aeruginosa* LpxA, it is not within hydrogen-bond distance to the ribose 3′-OH of the product (Figure 5C). Superimposition to the previously solved *L. interrogans* LpxA/product complex structure also suggests that acylated products bind similarly in both *L. interrogans* LpxA and *P. aeruginosa* LpxA (Figure 5D). Yet, different orientations for the 2-N acetyl group are observed when comparing the GlcNAc moiety in *P. aeruginosa* and the GlcNAc3N moiety in *L. interrogans* (Figure 5D). This difference may be due to the presence of Phe147, in place of Ile148 in *P. aeruginosa*, with the former being capable of reaching and establishing hydrophobic interactions with the apolar side of the 2-N acetyl group (Figure 5D). Additionally, Leu70 in *L. interrogans* has adopted an alternative conformation from the equivalent Leu71 in *P. aeruginosa* and would sterically clash with the 2-N acetyl conformation observed in the *P. aeruginosa* complex structure (Figure 5D). Another small difference is also observed in the orientation of the GlcNAc 6-OH, probably due to the presence of Gly71 instead of Lys in the *L. interrogans* ortholog, which is incapable of interacting with the GlcNAc 6-OH group (Figure 5D).

The major difference between the three orthologs, however, lies in the hydrophobic tunnel that accommodates the acyl chains of the acylated products and restricts their lengths (Figure 6). In lipid A biosynthesis, precise incorporation of specific hydrocarbon length acyl chains is highly conserved within a species, but it is divergent among different species. The term hydrocarbon ruler was first coined by Wyckoff et al. in describing residues that can act as precise measuring tools in *E. coli* and *P. aeruginosa* LpxA.[39] Such residues would disallow longer chains from binding due to steric clashes and would not provide sufficient hydrophobic interactions to shorter chains and therefore lose significant affinity. In *E. coli* LpxA, both structural and functional work support His191 acting as the hydrocarbon ruler, whereas in *L. interrogans* LpxA, it is Lys171. Mutational studies had suggested that Met169 serves the same role in *P. aeruginosa* LpxA and also showed how reciprocal mutations can completely reverse this selectivity between *E. coli* and *P. aeruginosa*.[39] The *E. coli* LpxA G173M mutant lost its preference for the 14C-long substrate while gaining activity for the 10C-long substrate; this resulted in a 10^6-fold selectivity switch from the C14 to the C10 substrate. Conversely, it was also shown that the M169G mutation in *P. aeruginosa* LpxA switched its specificity to the 14C-long product by 10^6-fold.[39] In *E. coli* LpxA, Gly173 lies in the same position as Met169 in *P. aeruginosa* LpxA.

The function of Met169 is now evident in our complex structure, and our results provide detailed structural information and support all previous functional findings. The LpxA/product complex reveals that product molecules with hydroxyacyl chains longer than 10 hydrocarbons would sterically clash with residue Met169, whereas shorter hydrocarbon chains would have reduced hydrophobic interactions with the pocket and therefore result in decreased affinity (Figures 5A,B and 6A). Superimposition of the *P. aeruginosa* LpxA with *E. coli* and *L. interrogans* LpxA complexes confirms that 14 and 12 hydrocarbon-long chains would clash with Met169 in the *P. aeruginosa* LpxA. Similarly, in *L. interrogans*

DOI: 10.1021/acs.biochem.5b00720
Biochemistry 2015, 54, 5937−5948

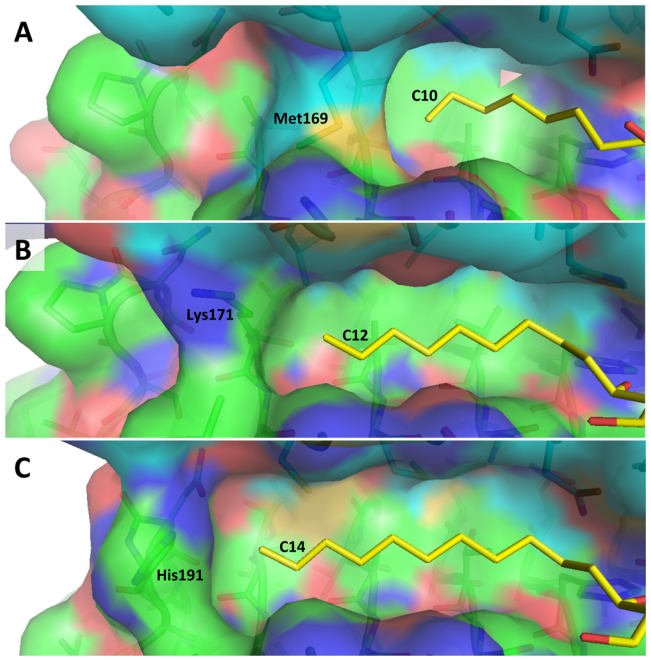

Figure 6. Acyl chain binding sites and hydrocarbon rulers. The two monomers at the dimer interface are colored cyan and green, respectively. Notice the hydrocarbon ruler is provided by a different monomer in *P. aeruginosa* LpxA in comparison to that in the other orthologs. (A) Surface model shows complementarity between the acyl chain and hydrophobic pocket in the *P. aeruginosa* LpxA/UDP-3-*O*-(*R*-3-hydroxydecanoyl)-GlcNAc complex structure and supports the role of Met169 as the hydrocarbon ruler. (B) *L. interrogans* LpxA complex shows Lys171 as the hydrocarbon ruler. (C) *E. coli* LpxA complex shows His191 as the hydrocarbon ruler.

LpxA, a hydroxyacyl chain longer than 12 hydrocarbons would clash with Lys171 (Figure 6B), and in *E. coli* LpxA, anything longer than a 14 hydrocarbon-long acyl chain would clash with His191 (Figure 6C). Interestingly, in these two LpxA structures, the hydrocarbon ruler (Lys171 and His191, respectively) resides on the same monomer as the catalytic histidine, whereas in *P. aeruginosa*, Met169 is provided in *trans* from a different monomer (Figures 5A,B and 6A) in comparison to His121. Also, since *P. aeruginosa* LpxA has Pro187 in the place of His191 from *E. coli* LpxA, no steric hindrance with the acyl chain would be expected at that site. It would be interesting, therefore, to determine what the longest hydrocarbon chain length is that could fit in the *P. aeruginosa* LpxA M169G mutant.

It has been previously proposed that the backbone amide group of a conserved Gly residue (Gly139 in *P. aeruginosa* LpxA) acts as the oxyanion hole by stabilizing the transition state during acylation of UDP-GlcNAc.[28,35] For that to occur in *P. aeruginosa* LpxA, the corresponding amide linker should be positioned in a way such that the carbonyl from the preceding Ala138 residue is orientated away from the active site and the backbone N of Gly139 is directed toward the active site, as observed in the *E. coli* and *L. interrogans* complex structures (backbone NH of residues Gly143 and Gly138, respectively) (Figure 7A,B) as well as in all other ortholog structures.[28,29,31−35] However, this conformation is not observed in the *P. aeruginosa* LpxA structure (Figure 7). Instead, the backbone N of Gly139 flips away from the active site, and the backbone carbonyl of Ala138 is oriented toward the ligand. Simulated annealing omit maps of this region in the apo (1.81 Å) (Figure 7C), substrate complex (2.16 Å), and product complex (2.30 Å) states all support the same conformational arrangement, which is most evident in the apo structure due to its higher resolution (Figure 7C). It also appears that the acyl chain carbonyl of UDP-3-*O*-(*R*-3-hydroxydecanoyl)-GlcNAc, which would normally interact with the oxyanion hole during the reaction, is directed away from the protein and toward the solvent (Figure 7A,B). In the *E. coli* (Figure 7A) and *L. interrogans* (Figure 7B) complex structures, the acyl chain carbonyl is positioned approximately within hydrogen-bond distance (3.3 Å) to the respective Gly residue, consistent with the role of the conserved Gly as the oxyanion hole (Figure 7A,B).

The favorable Gly backbone conformation, opposite to the one in our structures, has been observed not only in every additional LpxA ortholog structure but also in every LpxD structure solved to date.[49−52] The alternative conformation in our structures may have been due to increased flexibility of the Gly139 residue in *P. aeruginosa* LpxA. In *E. coli* LpxA, the peptide bond between Ala142 and Gly143, equivalent to Ala138 and Gly139 in *P. aeruginosa*, is stacked on top of the amide linkage between Ala124 and the catalytic histidine, His125. If the amide group adopts the same conformation as that observed in *P. aeruginosa* LpxA, then the backbone carbonyl group of Ala142 would clash with the Cβ atom of Ala124 in *E. coli* LpxA. In addition, the area that accommodates the acyl linkage appears to be wider in *P. aeruginosa* LpxA due to a substitution of Pro69 for the equivalent Gln73 in *E. coli* (Figure 7A). The distance between Gly139/Cα and Pro69/Cα is 10.8 Å in *P. aeruginosa* LpxA, in comparison to 8.3 Å between the corresponding atoms in *E. coli* LpxA. As a result, in the *P. aeruginosa* LpxA product complex, the acyl linkage is positioned farther away from Gly139 in order to form favorable interactions with Pro69. It is possible that the favorable Gly139 conformation, as observed in other LpxA structures, may be adopted by *P. aeruginosa* LpxA during catalysis, especially taking into consideration that our purified *P. aeruginosa* LpxA is biologically active (as tested in activity assays with the UDP-GlcNAc and acylated-ACP substrates; data not shown). In a recent *E. coli* LpxD-ACP complex (PDB ID: 4IHF),[53] the carbonyl group of the acyl chain, still attached to the 4′-phosphopantheteine group (4′-PPT) on the carrier protein, is pointed at the N group of the equivalent glycine residue and forms a hydrogen bond with a length of 3.1 Å, in comparison to 3.3 Å for the equivalent hydrogen bond in the *E. coli* LpxA product complex. This suggests that functional groups from ACP, such as 4′-PPT, can help to position the acyl chain carbonyl group for catalysis by interacting with the LpxA/LpxD active site. By placing the acyl chain carbonyl group close to Gly139, the binding of ACP may also induce the conformational change necessary to create the oxyanion hole.

CONCLUSIONS

P. aeruginosa, a pathogenic Gram-negative bacterium with a wide range of antibiotic resistance mechanisms, has been causing increasing public health concern.[4,5] Due to its importance in LPS synthesis, LpxA is a valuable target in drug discovery against *P. aeruginosa*.[7,16] Even though eight ortholog LpxA structures have been previously solved,[28−34] only three were in complex with glucosamine ligands and the *P. aeruginosa* LpxA structure was still lacking. Our X-ray structures reveal, for the first time, the architecture of *P. aeruginosa* LpxA and its detailed conformations in three different states. They

DOI: 10.1021/acs.biochem.5b00720
Biochemistry 2015, 54, 5937−5948

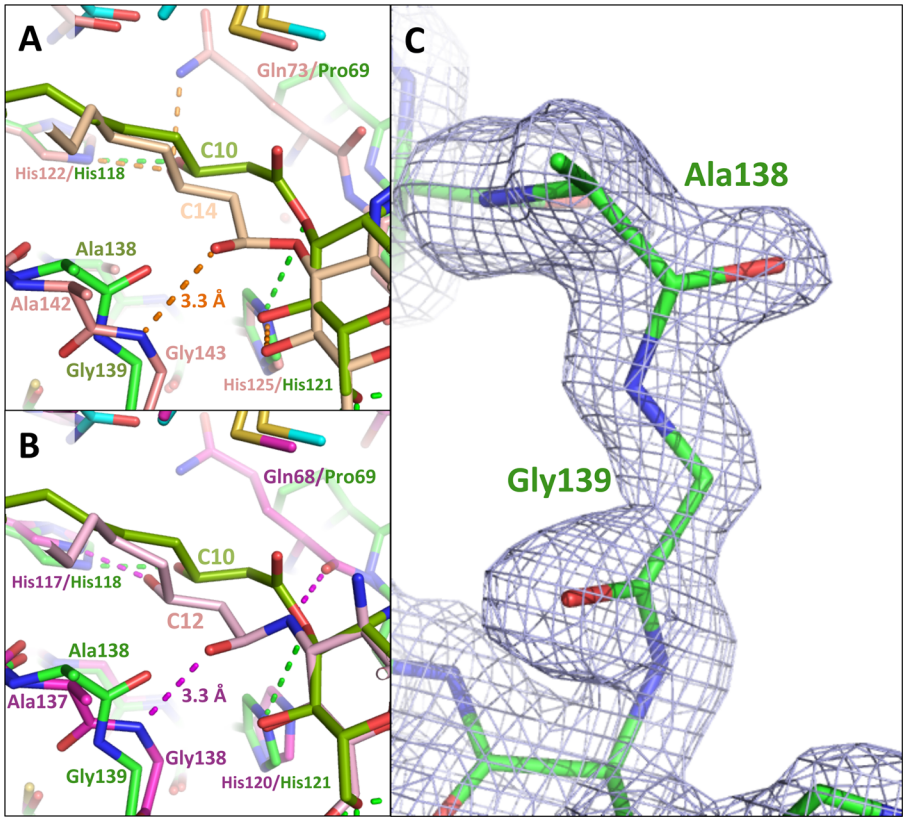

Figure 7. Alternative backbone conformation for highly conserved residues Ala138 and Gly139. (A) The *P. aeruginosa* LpxA/UDP-3-*O*-(*R*-3-hydroxydecanoyl)-GlcNAc (green/light green) complex superimposed to the *E. coli*/product complex structure (pink/light pink) shows opposing orientations for the protein backbone between highly conserved residues Ala138/142 and Gly139/143 and the potential hydrogen bonds. (B) The *P. aeruginosa* LpxA/UDP-3-*O*-(*R*-3-hydroxydecanoyl)-GlcNAc (green/light green) complex superimposed to the *L. interrogans*/product complex structure (purple/pink) shows opposing orientations for the protein backbone between highly conserved residues Ala138/137 and Gly139/138 and the potential hydrogen bonds. (C) Simulated annealing omit map created by omiting residues 132−144 in the apo *P. aeruginosa* LpxA structure (1.81 Å) and contoured at 3.0σ confirms that the backbone N of Gly139 is oriented away from the active site, whereas the backbone carbonyl of Ala138 is pointing toward the active site.

provide valuable information on the catalytic mechanism and substrate specificity of this protein, highlighting both the similarities to orthologs from other bacteria as well as the unique features of a hydrocarbon ruler and a flexible oxyanion hole. This information is also invaluable in employing a structure-based drug discovery approach that can lead to the discovery of new inhibitors against *P. aeruginosa* LpxA. Both the highly positively charged electrostatic features of the active site and the hydrophobic nature of the hydrocarbon chain cavity can be exploited simultaneously in designing molecules that will compete with the acylation of UDP-GlcNAc. Furthermore, considering the restricted depth of the hydrocarbon cavity governed by Met169 and the unique composition of certain active site residues, the design of potent molecules specific to the *P. aeruginosa* strain is indeed promising.

AUTHOR INFORMATION

Corresponding Author

*Phone: (813) 974-7809; Fax: (813) 974-7357; E-mail: ychen1@health.usf.edu.

Funding

This work was funded by a collaboration grant from Achaogen Inc.

Notes

The authors declare no competing financial interest.

ACKNOWLEDGMENTS

We would like to thank Dr. Ruslan Sanishvili from GM-CA CAT at the Advanced Photon Source (APS) for help with crystal analysis and the beamline scientists and staff at SER-CAT at APS for support with data collection. We thank Derek Nichols and Kyle Kroeck for reading the manuscript.

ABBREVIATIONS

ACP, acyl carrier protein; LβH, left-handed parallel beta-helix; LPS, lipopolysaccharide; LpxA, UDP-*N*-acetylglucosamine acyltransferase; RMSD, root-mean-square deviation; UDP-GlcNAc, uridine diphosphate *N*-acetylglucosamine

REFERENCES

(1) Tummler, B., Wiehlmann, L., Klockgether, J., and Cramer, N. (2014) Advances in understanding Pseudomonas. *F1000Prime Rep. 6*, 9.

(2) Morita, Y., Tomida, J., and Kawamura, Y. (2014) Responses of Pseudomonas aeruginosa to antimicrobials. *Front. Microbiol. 4*, 422.

(3) Bonomo, R. A., and Szabo, D. (2006) Mechanisms of multidrug resistance in Acinetobacter species and Pseudomonas aeruginosa. *Clin. Infect. Dis. 43*, S49−S56.

(4) Lister, P. D., Wolter, D. J., and Hanson, N. D. (2009) Antibacterial-resistant Pseudomonas aeruginosa: clinical impact and complex regulation of chromosomally encoded resistance mechanisms. *Clin Microbiol Rev. 22*, 582−610.

DOI: 10.1021/acs.biochem.5b00720
Biochemistry 2015, 54, 5937−5948

(5) Schurek, K. N., Breidenstein, E. B. M., and Hancock, R. E. W. (2012) Pseudomonas aeruginosa: a persistent pathogen in cystic fibrosis and hospital-associated infections, in *Antibiotic Discovery and Development* (Dougherty, T. J., and Pucci, M. J., Eds.) 1st ed., pp 679–715, Springer, New York.
(6) Wolska, K., Kot, B., Piechota, M., and Frankowska, A. (2013) [Resistance of Pseudomonas aeruginosa to antibiotics]. *Postepy Hig Med. Dosw (Online) 67*, 1300–1311.
(7) Rusmini, R., Vecchietti, D., Macchi, R., Vidal-Aroca, F., and Bertoni, G. (2014) A shotgun antisense approach to the identification of novel essential genes in Pseudomonas aeruginosa. *BMC Microbiol. 14*, 24.
(8) Wang, X., and Quinn, P. J. (2010) Lipopolysaccharide: Biosynthetic pathway and structure modification. *Prog. Lipid Res. 49*, 97–107.
(9) King, J. D., Kocincova, D., Westman, E. L., and Lam, J. S. (2009) Review: Lipopolysaccharide biosynthesis in Pseudomonas aeruginosa. *Innate Immun. 15*, 261–312.
(10) Heine, H., Rietschel, E. T., and Ulmer, A. J. (2001) The biology of endotoxin. *Mol. Biotechnol. 19*, 279–296.
(11) Raetz, C. R. (1993) Bacterial endotoxins: extraordinary lipids that activate eucaryotic signal transduction. *J. Bacteriol. 175*, 5745–5753.
(12) Raetz, C. R., and Whitfield, C. (2002) Lipopolysaccharide endotoxins. *Annu. Rev. Biochem. 71*, 635–700.
(13) Lam, J. S., Taylor, V. L., Islam, S. T., Hao, Y., and Kocincova, D. (2011) Genetic and Functional Diversity of Pseudomonas aeruginosa Lipopolysaccharide. *Front. Microbiol. 2*, 118.
(14) Kocincova, D., and Lam, J. S. (2011) Structural diversity of the core oligosaccharide domain of Pseudomonas aeruginosa lipopolysaccharide. *Biochemistry (Moscow) 76*, 755–760.
(15) Raetz, C. R., Reynolds, C. M., Trent, M. S., and Bishop, R. E. (2007) Lipid A modification systems in gram-negative bacteria. *Annu. Rev. Biochem. 76*, 295–329.
(16) Galloway, S. M., and Raetz, C. R. (1990) A mutant of Escherichia coli defective in the first step of endotoxin biosynthesis. *J. Biol. Chem. 265*, 6394–6402.
(17) Anderson, M. S., and Raetz, C. R. (1987) Biosynthesis of lipid A precursors in Escherichia coli. A cytoplasmic acyltransferase that converts UDP-N-acetylglucosamine to UDP-3-O-(R-3-hydroxymyristoyl)-N-acetylglucosamine. *J. Biol. Chem. 262*, 5159–5169.
(18) Anderson, M. S., Bull, H. G., Galloway, S. M., Kelly, T. M., Mohan, S., Radika, K., and Raetz, C. R. (1993) UDP-N-acetylglucosamine acyltransferase of Escherichia coli. The first step of endotoxin biosynthesis is thermodynamically unfavorable. *J. Biol. Chem. 268*, 19858–19865.
(19) Young, K., Silver, L. L., Bramhill, D., Cameron, P., Eveland, S. S., Raetz, C. R., Hyland, S. A., and Anderson, M. S. (1995) The envA permeability/cell division gene of Escherichia coli encodes the second enzyme of lipid A biosynthesis. UDP-3-O-(R-3-hydroxymyristoyl)-N-acetylglucosamine deacetylase. *J. Biol. Chem. 270*, 30384–30391.
(20) Bartling, C. M., and Raetz, C. R. (2008) Steady-state kinetics and mechanism of LpxD, the N-acyltransferase of lipid A biosynthesis. *Biochemistry 47*, 5290–5302.
(21) Raetz, C. R., Guan, Z., Ingram, B. O., Six, D. A., Song, F., Wang, X., and Zhao, J. (2008) Discovery of new biosynthetic pathways: the lipid A story. *J. Lipid Res. 50*, S103–S108.
(22) Vaara, M. (1996) Lipid A: target for antibacterial drugs. *Science 274*, 939–940.
(23) Onishi, H. R., Pelak, B. A., Gerckens, L. S., Silver, L. L., Kahan, F. M., Chen, M. H., Patchett, A. A., Galloway, S. M., Hyland, S. A., Anderson, M. S., and Raetz, C. R. (1996) Antibacterial agents that inhibit lipid A biosynthesis. *Science 274*, 980–982.
(24) Williams, A. H., Immormino, R. M., Gewirth, D. T., and Raetz, C. R. (2006) Structure of UDP-N-acetylglucosamine acyltransferase with a bound antibacterial pentadecapeptide. *Proc. Natl. Acad. Sci. U. S. A. 103*, 10877–10882.
(25) Jenkins, R. J., and Dotson, G. D. (2012) Dual targeting antibacterial peptide inhibitor of early lipid A biosynthesis. *ACS Chem. Biol. 7*, 1170–1177.
(26) Dotson, G. D., Kaltashov, I. A., Cotter, R. J., and Raetz, C. R. (1998) Expression cloning of a Pseudomonas gene encoding a hydroxydecanoyl-acyl carrier protein-dependent UDP-GlcNAc acyltransferase. *J. Bacteriol. 180*, 330–337.
(27) Pfitzner, U., Raetz, C. R., and Roderick, S. L. (1995) Crystallization of UDP-N-acetylglucosamine O-acyltransferase from Escherichia coli. *Proteins: Struct., Funct., Genet. 22*, 191–192.
(28) Robins, L. I., Williams, A. H., and Raetz, C. R. (2009) Structural basis for the sugar nucleotide and acyl-chain selectivity of Leptospira interrogans LpxA. *Biochemistry 48*, 6191–6201.
(29) Badger, J., Chie-Leon, B., Logan, C., Sridhar, V., Sankaran, B., Zwart, P. H., and Nienaber, V. (2012) Structure determination of LpxA from the lipopolysaccharide-synthesis pathway of Acinetobacter baumannii. *Acta Crystallogr., Sect. F: Struct. Biol. Cryst. Commun. 68*, 1477–1481.
(30) Raetz, C. R., and Roderick, S. L. (1995) A left-handed parallel beta helix in the structure of UDP-N-acetylglucosamine acyltransferase. *Science 270*, 997–1000.
(31) Lee, B. I., and Suh, S. W. (2003) Crystal structure of UDP-N-acetylglucosamine acyltransferase from Helicobacter pylori. *Proteins: Struct., Funct., Genet. 53*, 772–774.
(32) Baugh, L., Gallagher, L. A., Patrapuvich, R., Clifton, M. C., Gardberg, A. S., Edwards, T. E., Armour, B., Begley, D. W., Dieterich, S. H., Dranow, D. M., Abendroth, J., Fairman, J. W., Fox, D., 3rd, Staker, B. L., Phan, I., Gillespie, A., Choi, R., Nakazawa-Hewitt, S., Nguyen, M. T., Napuli, A., Barrett, L., Buchko, G. W., Stacy, R., Myler, P. J., Stewart, L. J., Manoil, C., and Van Voorhis, W. C. (2013) Combining functional and structural genomics to sample the essential Burkholderia structome. *PLoS One 8*, e53851.
(33) Joo, S. H., Chung, H. S., Raetz, C. R., and Garrett, T. A. (2012) Activity and crystal structure of Arabidopsis thaliana UDP-N-acetylglucosamine acyltransferase. *Biochemistry 51*, 4322–4330.
(34) Ngo, A., Fong, K. T., Cox, D. L., Chen, X., and Fisher, A. J. (2015) Structures of Bacteroides fragilis uridine 5′-diphosphate-N-acetylglucosamine (UDP-GlcNAc) acyltransferase (BfLpxA). *Acta Crystallogr., Sect. D: Biol. Crystallogr. 71*, 1068–1076.
(35) Williams, A. H., and Raetz, C. R. (2007) Structural basis for the acyl chain selectivity and mechanism of UDP-N-acetylglucosamine acyltransferase. *Proc. Natl. Acad. Sci. U. S. A. 104*, 13543–13550.
(36) Wyckoff, T. J., and Raetz, C. R. (1999) The active site of Escherichia coli UDP-N-acetylglucosamine acyltransferase. Chemical modification and site-directed mutagenesis. *J. Biol. Chem. 274*, 27047–27055.
(37) Williamson, J. M., Anderson, M. S., and Raetz, C. R. (1991) Acyl-acyl carrier protein specificity of UDP-GlcNAc acyltransferases from gram-negative bacteria: relationship to lipid A structure. *J. Bacteriol. 173*, 3591–3596.
(38) Odegaard, T. J., Kaltashov, I. A., Cotter, R. J., Steeghs, L., van der Ley, P., Khan, S., Maskell, D. J., and Raetz, C. R. (1997) Shortened hydroxyacyl chains on lipid A of Escherichia coli cells expressing a foreign UDP-N-acetylglucosamine O-acyltransferase. *J. Biol. Chem. 272*, 19688–19696.
(39) Wyckoff, T. J., Lin, S., Cotter, R. J., Dotson, G. D., and Raetz, C. R. (1998) Hydrocarbon rulers in UDP-N-acetylglucosamine acyltransferases. *J. Biol. Chem. 273*, 32369–32372.
(40) Otwinowski, Z., and Minor, W. (1997) Processing of X-ray diffraction data collected in oscillation mode. *Methods Enzymol. 276*, 307–326.
(41) Vagin, A., and Teplyakov, A. (2010) Molecular replacement with MOLREP. *Acta Crystallogr., Sect. D: Biol. Crystallogr. 66*, 22–25.
(42) Winn, M. D., Ballard, C. C., Cowtan, K. D., Dodson, E. J., Emsley, P., Evans, P. R., Keegan, R. M., Krissinel, E. B., Leslie, A. G., McCoy, A., McNicholas, S. J., Murshudov, G. N., Pannu, N. S., Potterton, E. A., Powell, H. R., Read, R. J., Vagin, A., and Wilson, K. S. (2011) Overview of the CCP4 suite and current developments. *Acta Crystallogr., Sect. D: Biol. Crystallogr. 67*, 235–242.

DOI: 10.1021/acs.biochem.5b00720
Biochemistry 2015, 54, 5937–5948

(43) Eswar, N., Webb, B., Marti-Renom, M. A., Madhusudhan, M. S., Eramian, D., Shen, M. Y., Pieper, U., and Sali, A. (2007) Comparative protein structure modeling using MODELLER. *Current Protocols in Protein Science*, DOI: 10.1002/0471140864.ps0209s50.
(44) Emsley, P., and Cowtan, K. (2004) Coot: model-building tools for molecular graphics. *Acta Crystallogr., Sect. D: Biol. Crystallogr. 60*, 2126−2132.
(45) Adams, P. D., Afonine, P. V., Bunkoczi, G., Chen, V. B., Davis, I. W., Echols, N., Headd, J. J., Hung, L. W., Kapral, G. J., Grosse-Kunstleve, R. W., McCoy, A. J., Moriarty, N. W., Oeffner, R., Read, R. J., Richardson, D. C., Richardson, J. S., Terwilliger, T. C., and Zwart, P. H. (2010) PHENIX: a comprehensive Python-based system for macromolecular structure solution. *Acta Crystallogr., Sect. D: Biol. Crystallogr. 66*, 213−221.
(46) Vagin, A. A., Steiner, R. A., Lebedev, A. A., Potterton, L., McNicholas, S., Long, F., and Murshudov, G. N. (2004) REFMAC5 dictionary: organization of prior chemical knowledge and guidelines for its use. *Acta Crystallogr., Sect. D: Biol. Crystallogr. 60*, 2184−2195.
(47) *The PyMOL Molecular Graphics System*, version 1.3, Schrödinger, LLC, New York.
(48) Ulaganathan, V., Buetow, L., and Hunter, W. N. (2007) Nucleotide substrate recognition by UDP-N-acetylglucosamine acyltransferase (LpxA) in the first step of lipid A biosynthesis. *J. Mol. Biol. 369*, 305−312.
(49) Bartling, C. M., and Raetz, C. R. (2009) Crystal structure and acyl chain selectivity of Escherichia coli LpxD, the N-acyltransferase of lipid A biosynthesis. *Biochemistry 48*, 8672−8683.
(50) Buetow, L., Smith, T. K., Dawson, A., Fyffe, S., and Hunter, W. N. (2007) Structure and reactivity of LpxD, the N-acyltransferase of lipid A biosynthesis. *Proc. Natl. Acad. Sci. U. S. A. 104*, 4321−4326.
(51) Badger, J., Chie-Leon, B., Logan, C., Sridhar, V., Sankaran, B., Zwart, P. H., and Nienaber, V. (2011) The structure of LpxD from Pseudomonas aeruginosa at 1.3 A resolution. *Acta Crystallogr., Sect. F: Struct. Biol. Cryst. Commun. 67*, 749−752.
(52) Badger, J., Chie-Leon, B., Logan, C., Sridhar, V., Sankaran, B., Zwart, P. H., and Nienaber, V. (2013) Structure determination of LpxD from the lipopolysaccharide-synthesis pathway of Acinetobacter baumannii. *Acta Crystallogr., Sect. F: Struct. Biol. Cryst. Commun. 69*, 6−9.
(53) Masoudi, A., Raetz, C. R., Zhou, P., and Pemble, C. W., IV (2013) Chasing acyl carrier protein through a catalytic cycle of lipid A production. *Nature 505*, 422−426.

DOI: 10.1021/acs.biochem.5b00720
Biochemistry 2015, 54, 5937−5948